

1 Geochemistry and petrography of martian meteorite Northwest Africa 11115: A rare earth element-enriched  
2 olivine-phyric shergottite closely linked to Northwest Africa 1068

3  
4 M. Melwani Daswani<sup>a\*,+</sup>, N. D. Greber<sup>b, c</sup>, Jinping Hu<sup>d</sup>, R. C. Greenwood<sup>e</sup>, and P. R. Heck<sup>a, f</sup>

5  
6 <sup>a</sup> Department of the Geophysical Sciences and Chicago Center for Cosmochemistry, University of Chicago,  
7 Chicago, IL 60637, USA.

8 <sup>b</sup> Natural History Museum of Geneva, Route de Malagnou 1, 1208, Geneva, Switzerland

9 <sup>c</sup> Institute of Geological Sciences, University of Bern, Baltzerstrasse 1+3, 3012 Bern, Switzerland

10 <sup>d</sup> Division of Geological and Planetary Sciences, California Institute of Technology, 1200 E. California Blvd.  
11 M/C170-25, Pasadena, CA, 91125, USA.

12 <sup>e</sup> Planetary and Space Sciences, The Open University, Walton Hall, Milton Keynes, MK7 6AA, UK.

13 <sup>f</sup> Robert A. Pritzker Center for Meteoritics and Polar Studies, Negaunee Integrative Research Center, The Field  
14 Museum of Natural History, Chicago, IL 60605, USA.

15  
16 \* Corresponding author ([mohit.melwani.daswani@jpl.nasa.gov](mailto:mohit.melwani.daswani@jpl.nasa.gov))

17 <sup>+</sup> Now at the Jet Propulsion Laboratory, California Institute of Technology, 4800 Oak Grove Dr. Pasadena, CA  
18 91109, USA.

19  
20  
21 **Abstract**

22 The shergottite family of meteorites shows a remarkable petrographic and geochemical variety, revealing  
23 information about mantle processes and basalt formation on Mars. Northwest Africa (NWA) 11115, found in  
24 Morocco in 2016, is one of the newest meteorites in this family. We report bulk-rock major and trace element  
25 abundances of NWA 11115, bulk oxygen isotope systematics, and the petrography and mineralogy of a thick  
26 section, and compare the geochemistry of this recent find to other martian rocks. NWA 11115 is an olivine-  
27 phyric shergottite with an enriched rare earth element pattern, and shares similarities with NWA 1068, another  
28 enriched olivine-phyric shergottite. The large (< 2.5 mm) olivine phenocrysts are likely to be cumulates, similar  
29 to NWA 1068. However, the abundant maskelynite (~30 vol. %) in NWA 11115 places the bulk chemistry  
30 somewhat closer to the basaltic shergottites. We suggest that NWA 11115 is genetically linked to NWA 1068,  
31 perhaps crystallizing slightly above in the same cumulate pile. NWA 11115 contains one of the lowest K/Th  
32 ratios among the martian meteorites ( $K/Th = 2987 \pm 810$ ), and far lower than the surface of Mars ( $K/Th =$   
33  $5300$ ). Finally, while NWA 11115 contains abundant (~0.4 vol. %) fracture-filling calcite (presumably from  
34 hot desert alteration during its terrestrial residence), diagnostic bulk element mass ratios were not indicative  
35 of the presence of terrestrial alteration ( $Th/U \approx 4.09$ ,  $Sr/Nd \approx 12.26$ ,  $K/La \approx 526.94$ ,  $Ce/Ce^* \approx 1.01$ ).

36

## 37 1. INTRODUCTION

38 Northwest Africa (NWA) 11115 is a martian shergottite meteorite found at an undisclosed location in  
39 Morocco in 2016. A 34.2 g aliquot of the main mass (246.76 g) was donated to the Field Museum of Natural  
40 History (FMNH) in Chicago by T. Boudreaux, and its official name was approved in February 2017 (The  
41 Meteoritical Society 2017). Here, we describe the geochemistry, mineralogy and petrography of NWA 11115  
42 in relation to other martian meteorites and the surface of Mars, we use oxygen isotope systematics to confirm  
43 its provenance, and we show that it belongs to the uncommon group of rare earth element (REE) enriched  
44 olivine-phyric shergottites.

45

46 In the following work, we provide a general introduction to the shergottite meteorites to provide context  
47 for the study of NWA 11115. We then explain the analytical methods used to study chemical composition,  
48 oxygen isotopes, mineralogy and petrography of NWA 11115 in §2, and then report the detailed results of the  
49 analyses in §3. In §4, we discuss and interpret the results, focusing on the provenance of NWA 11115 and its  
50 relationship to other shergottites, and the evidence for terrestrial weathering. Finally, we provide our  
51 conclusions and suggestions for further study of NWA 11115 in §5.

52

### 53 1.1. Shergottites: a primer

54 Martian meteorites probe the chemistry of the interior of Mars, and complement the analyses and  
55 discoveries carried out by landed and orbiting spacecraft. The petrologic and geochemical properties of martian  
56 materials are characteristic of specific geologic processes that occurred on Mars and can, for example, inform  
57 about the degree of magmatic differentiation, volcanism, aqueous alteration and the effects of impact.  
58 Therefore, every martian meteorite recovered is scientifically significant in that it can help unravel a portion  
59 of Mars' geologic history. Until samples are returned from Mars, the only martian rocks physically available  
60 for study in terrestrial laboratories are meteorites. Of the 152 currently named martian meteorites, the  
61 shergottites are the most numerous group, comprising 132 rocks as of May 2021, not counting paired rocks,  
62 i.e. fragments belonging to the same meteor (Irving 2021). The shergottites' geochemical, mineralogic and  
63 petrographic characteristics have informed about the composition of the martian mantle, crust and atmosphere,  
64 and about igneous processes and the formation of basalts on Mars.

65 Petrographically and mineralogically, the shergottites are broadly divided into the olivine-phyric, poikilitic  
66 (formerly lherzolitic), and pyroxene-phyric/basaltic groups (e.g., Goodrich 2002; Papike et al. 2009). The  
67 olivine-phyric shergottites (e.g. NWA 2990, Tissint and Yamato 980459) are related by their olivine-porphyratic  
68 textures within finer-grained groundmass, with low augite contents, and with chromite in addition to Fe-Ti  
69 oxides. The olivine-phyric shergottites represent rocks that crystallized from melt (e.g. Y-980459) or that  
70 contain olivine crystal cumulates (Filiberto and Dasgupta 2011; e.g., Usui et al. 2008). The poikilitic  
71 shergottites (e.g. Allan Hills 77005 and NWA 2646) are coarse-grained and the most olivine-rich (~30 – 60  
72 vol. % olivine) of the shergottites. They additionally contain pyroxene, chromite and maskelynite, and are  
73 likely cumulates (e.g., Goodrich 2002; Papike et al. 2009). On the other hand, the pyroxene-phyric/basaltic

74 meteorites (e.g. Zagami, Shergotty, NWA 7032, NWA 7635 and NWA 8159) are a diverse group containing  
75 almost no olivine and chromite, but instead are almost entirely formed of augite, pigeonite and maskelynite,  
76 and vary widely in their grain size, probably as a result of different cooling rates within lavas (e.g. Goodrich,  
77 2002; Papike et al., 2009). Finally, polymict breccia NWA 7034 and its pairs contain numerous matrix-  
78 supported clasts of varying petrologic types and compositions that match the shergottite lithologies (e.g. Agee  
79 et al., 2013; Humayun et al., 2013; Wittmann et al., 2015; Santos et al., 2015).

80 Separate from their petrologic grouping, shergottites are also divided geochemically into the light rare-earth  
81 element (LREE) enriched, intermediate, and depleted groups (e.g. McSween, 1994; Filiberto, 2017), relative  
82 to the abundance of their heavy REE (HREE), and CI chondrite REE concentrations. Enriched shergottites  
83 (e.g. Shergotty and NWA 4468) have moderately flat REE abundance profiles with no significant enrichments  
84 or depletions in any specific REE ( $La/Yb > 0.7$ ). However, their REE abundances are all  $\sim 10 \times$  enriched  
85 relative to CI chondrites, most likely as a result of subsolidus equilibration, melt fractionation and assimilation  
86 from crustal sources (e.g. Treiman, 1996; Borg and Draper, 2003; Papike et al., 2009). Depleted shergottites  
87 (e.g. NWA 7032 and Tissint) have significantly different LREE concentrations relative to their HREE  
88 abundances ( $La/Yb < 0.3$ ), and the LREE tend to be depleted compared to CI chondrites ( $LREE < 1 \times CI$   
89 chondrite LREE). Finally, the intermediate shergottites are somewhat more enriched in HREE relative to LREE  
90 ( $0.3 < La/Yb < 0.7$ ), and their overall REE abundances are somewhat elevated compared to CI chondrites ( $1 -$   
91  $10 \times CI$  chondrite REE) (e.g. Papike et al., 2009; Taylor, 2013).

92

## 93 2. ANALYTICAL METHODS

### 94 2.1. X-ray computed tomography

95 Before cutting, the complete specimen of NWA 11115 was scanned using X-ray computer tomography  
96 (CT) with a GE v|tome|x s 240 scanner at the University of Chicago's PaleoCT lab. X-ray CT enabled us to  
97 quantify the porosity of the meteorite and the interconnectivity of the pores. We used a voltage of 190 kV and  
98 a current of 150  $\mu A$  at a voxel size of 30.3  $\mu m$ ; a 0.5 mm Sn filter was used. The total scan time was 6 hours  
99 43 minutes. The scan was performed in several segments that were stitched together in the reconstruction. We  
100 used the *Fiji* distribution of the *ImageJ* software (Schindelin et al. 2012) to analyze the tomographic dataset.  
101 The tomographic reconstruction is available in the electronic appendix.

102

### 103 2.2. Mineralogy and petrography using electron microscopy

104 A chip of NWA 1115 was cut using water-free high-purity (Optima™) isopropanol with a low-speed  
105 Buehler IsoMet wafering saw outfitted with a thin diamond blade. The chip was embedded in a 1-inch diameter  
106 epoxy round (Buehler EpoxiCure® 2; pre-2016 formulation), polished with diamond film and water-free  
107 Optima™ isopropanol, and coated with carbon for characterization by electron microscopy. The sample was  
108 analyzed at the FMNH with a Zeiss EVO 60 Scanning Electron Microscope (SEM) equipped with an Oxford  
109 Instruments X-Max 50 silicon drift detector, and at the University of Chicago with a TESCAN LYRA3 FIB-

110 SEM equipped with two Oxford Instruments X-Max-80 silicon drift detectors. Quantitative analyses of the  
111 mineral compositions, backscattered electron (BSE) and elemental mapping were carried out with Oxford  
112 Instruments energy dispersive spectroscopy (EDS) systems attached to both SEMs, with a 15 kV acceleration  
113 voltage and a beam current of ~2-4 nA. We used a set of mineral reference standards to calibrate the EDS, and  
114 calibrated and monitored stability of the e-beam current by using bracketed analyses of a Cu standard in  
115 between 10 – 20 sample spots. We report only compositions that give total weights of  $100 \pm 2$  wt. %. Oxford  
116 Instruments' *AZtec* software was used to produce the raw BSE and element map images; *Fiji* and the *GNU*  
117 *Image Manipulation Program* (GIMP) were used to produce image composites, for mineral phase mapping  
118 and for modal mineralogy.

119

### 120 *2.2.1. Bulk composition using LA-ICP-MS*

121

122 Around 0.462 g of NWA 11115 were milled with an agate mortar to measure major and trace elements by  
123 LA-ICP-MS on “Pressed Powder Pellets” following the protocol of Peters and Pettke (2017) at the University  
124 of Bern. The USGS glass standard GSD-1G was used for instrument calibration. To check the accuracy of the  
125 analyses the basaltic reference glass KL2-G was measured three times before and after the analyses of the  
126 unknowns. Due to limited sample availability, we were not able to produce a powder with a grain size of below  
127 5  $\mu\text{m}$ , and certain elements like Cr and  $\text{P}_2\text{O}_5$  might thus be subjected to nugget effects (due to chromite and  
128 apatite, respectively). Therefore, to obtain a representative average of the major and trace element  
129 concentration of NWA 11115 we performed 27 consecutive analyses. Except for Cr, the mean and median  
130 values of the 27 individual analyses agree to around  $\pm 5$  % with each other, indicating that our data is  
131 representative of the bulk rock. In addition, Se concentrations measured in the KL2-G standard differed from  
132 the values reported in literature, so we consider the Se concentrations measured in NWA 11115 to be uncertain  
133 and report them only in the Supplementary Spreadsheet File S1. We note that we reported preliminary bulk  
134 geochemical analyses of this meteorite (Melwani Daswani et al. 2017), but that those results were likely  
135 contaminated or affected by the sample preparation procedure. The results we report below are the authoritative  
136 version. We include the sidelined analyses in the Supplementary Information for comparison and completion.

137

### 138 *2.2.2. Oxygen isotope systematics using laser fluorination*

139 The oxygen isotopic composition of NWA 11115 was determined by infrared laser-assisted fluorination at the  
140 Open University on two aliquots of homogenized powder each weighing ~2 mg (Greenwood et al. 2017;  
141 Miller et al. 1999) at the Open University. These were loaded into a Ni sample block along with obsidian  
142 internal standards. The sample block was then positioned into a two-part chamber, made vacuum tight using a  
143 compression seal fitted with a copper gasket and clamped by a quick-release KFX clamp (Greenwood et al.  
144 2017; Miller et al. 1999). Following loading, the cell was heated under vacuum for a minimum of 24 hours to  
145 a temperature in excess of 70 °C so as to remove any adsorbed atmospheric moisture. Prior to fluorination, the

146 system blank was systematically reduced by flushing the chamber with aliquots of BrF<sub>5</sub>, with the final blank  
147 being less than 60 nmol O<sub>2</sub>. Sample heating in the presence of BrF<sub>5</sub> was carried out using an integrated 50 W  
148 infrared CO<sub>2</sub> laser (10.6 μm) and video system mounted on an X-Y-Z gantry supplied by Photon Machines Inc.  
149 (Greenwood et al., 2017). After fluorination, the released O<sub>2</sub> was purified by passing it through two cryogenic  
150 (liquid nitrogen) traps and over a bed of heated KBr. The isotopic composition of the purified oxygen was  
151 analyzed using a Thermo Fisher MAT 253 dual inlet mass spectrometer (mass resolving power 200).  
152 Interference at m/z = 33 by NF<sup>+</sup> was monitored by performing scans for NF<sub>2</sub><sup>+</sup> on the sample gas before  
153 analyzing each sample; this was below interference levels during the analyses reported here. Our current  
154 system precision based on repeat analyses (N = 39) of our obsidian internal standard is: ± 0.052 ‰ for δ<sup>17</sup>O;  
155 ± 0.094 ‰ for δ<sup>18</sup>O; ± 0.017 ‰ for Δ<sup>17</sup>O (2σ) (Starkey et al. 2016).  
156 Oxygen isotopic analyses are reported in standard δ notation, where δ<sup>18</sup>O has been calculated as: δ<sup>18</sup>O =  
157 [(<sup>18</sup>O/<sup>16</sup>O<sub>sample</sub>/<sup>18</sup>O/<sup>16</sup>O<sub>ref</sub>) - 1] × 1000 (‰) and, similarly, for δ<sup>17</sup>O using the <sup>17</sup>O/<sup>16</sup>O ratio. In order to compare  
158 our results with other published laser fluorination analyses of martian samples we have calculated Δ<sup>17</sup>O, which  
159 represents the deviation from the terrestrial fractionation line, as Δ<sup>17</sup>O = δ<sup>17</sup>O - 0.52 × δ<sup>18</sup>O.

160

### 161 3. RESULTS

#### 162 3.1. Petrography and mineralogy

163 The 1-inch round polished thick section of NWA 11115 consists of about 4 % pore space. We report the  
164 porosity-removed modal mineralogy: olivine forms approximately 14 %, pyroxene (mainly pigeonite) forms  
165 ~ 50 %, and plagioclase (as maskelynite) around ~ 30 %. The remainder consists of ~ 0.3 % sulfides, ~ 0.3 %  
166 orthopyroxene, ~ 2 % Fe-Ti-Cr-oxides, ~ 2 % phosphates, and trace K-feldspar and silica (Figure 1). Abundant  
167 (~ 0.4 %) secondary Mg-rich calcite (almost certainly produced by terrestrial fluids) infills pores, especially  
168 within the numerous cracks in and around olivine grains. Most mineral phases are medium grained and  
169 subhedral, except for sulfides and Fe-oxides, which are fine-grained. Olivine crystals up to 2.5 mm across are  
170 visible, along with elongated grains of pyroxene of about the same length. Maskelynite infills the interstices  
171 between grains, and mineral grains follow no preferential orientation. Also visible within the section are  
172 numerous shock melt pockets of mixed pyroxene and feldspathic glass. Overall, the large grain size of the  
173 olivine and pyroxene in the sample is consistent with martian gabbros (e.g. NWA 6963; Filiberto et al., 2014)  
174 rather than typical olivine-phyric shergottites, whose olivine grains are significantly larger than the remaining  
175 mineral phases (mostly pyroxene and plagioclase), and which form a fine-grained groundmass or matrix (e.g.  
176 NWA 6234/2990; Gross et al., 2013). However, the modal mineralogy of NWA 11115 lies between pyroxene-  
177 phyric/basaltic and olivine-phyric shergottites, i.e. it contains significant amounts of plagioclase, but also  
178 contains olivine. The tomographic reconstruction shows the same lithology throughout the complete sample  
179 of NWA 11115 (electronic appendix), thus, we infer that the polished section is a representative sample of the  
180 entire rock. Average compositions of the main mineral phases are shown in Table 1.

181

182

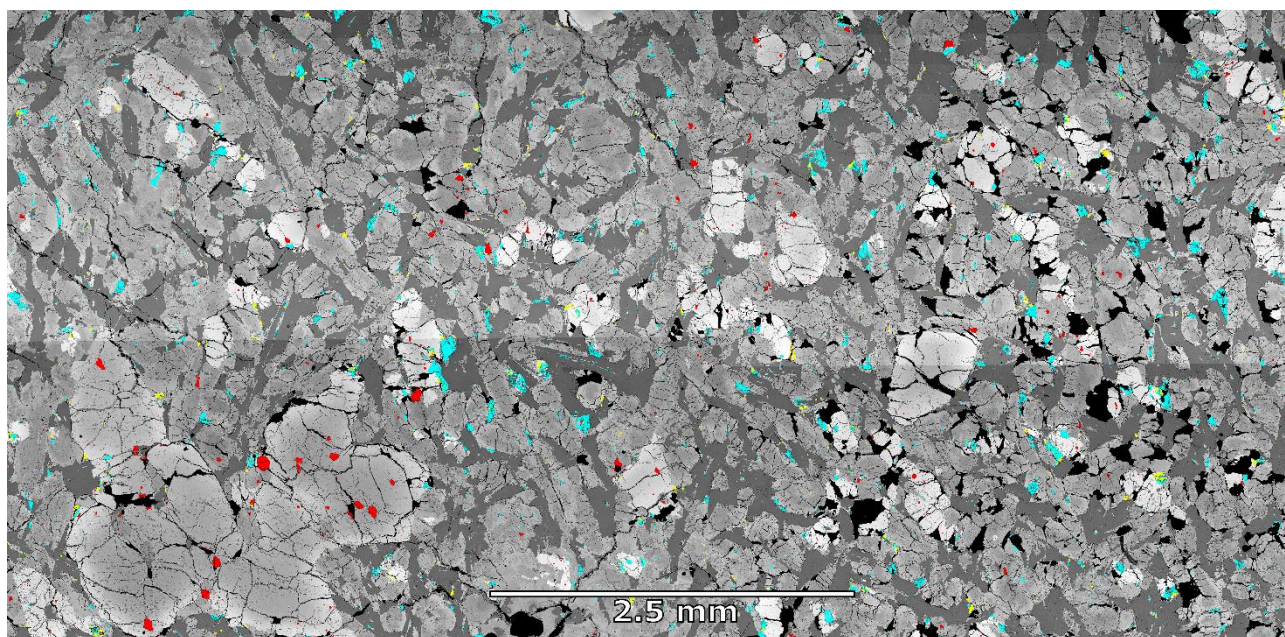


Figure 1. BSE image mosaic of a representative section of NWA 11115. Refractory phases are colored in the image in order to distinguish them: chromite grains are red, ilmenite grains are blue, and sulfides are yellow. Black areas are secondary pores and fractures.

183

Table 1. Average major oxide concentrations of the major phases in the thick section.

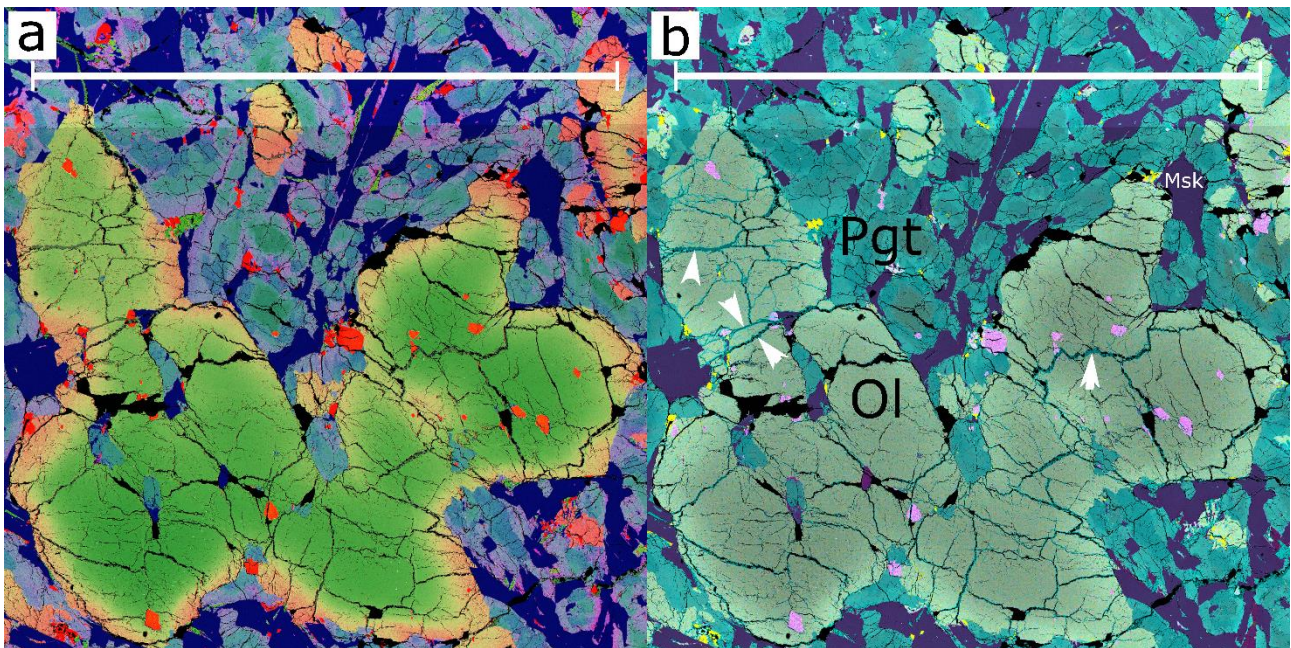
|                                | <sup>a</sup> Olivine |               | <sup>b</sup> Pigeonite |               | Enstatite        |               | Augite |               | Maskelynite |               |
|--------------------------------|----------------------|---------------|------------------------|---------------|------------------|---------------|--------|---------------|-------------|---------------|
|                                | N = 57               |               | N = 24                 |               | N = 8            |               | N = 2  |               | N = 74      |               |
|                                | Wt. %                | $\pm 1\sigma$ | Wt. %                  | $\pm 1\sigma$ | Wt. %            | $\pm 1\sigma$ | Wt. %  | $\pm 1\sigma$ | Wt. %       | $\pm 1\sigma$ |
| SiO <sub>2</sub>               | 34.68                | 1.91          | 51.60                  | 1.07          | 53.95            | 0.42          | 21.22  | 0.54          | 55.81       | 1.22          |
| TiO <sub>2</sub>               | nd <sup>c</sup>      | -             | 0.22                   | 0.17          | bdl <sup>d</sup> | -             | 0.37   | 0.04          | bdl         | 0.03          |
| Al <sub>2</sub> O <sub>3</sub> | nd                   | -             | 1.54                   | 0.33          | 0.45             | 0.20          | 1.54   | 0.33          | 27.10       | 0.81          |
| Cr <sub>2</sub> O <sub>3</sub> | nd                   | -             | 0.40                   | 0.19          | 0.41             | 0.06          | 0.63   | 0.02          | nd          | -             |
| FeO <sub>T</sub> <sup>e</sup>  | 41.00                | 9.35          | 20.94                  | 3.28          | 16.49            | 0.27          | 17.14  | 2.32          | 0.76        | 0.17          |
| MnO                            | 0.78                 | 0.18          | 0.69                   | 0.14          | 0.58             | 0.06          | 0.60   | 0.01          | nd          | -             |
| MgO                            | 22.71                | 7.87          | 18.60                  | 3.02          | 25.03            | 0.31          | 16.09  | 1.01          | 0.02        | 0.05          |
| CaO                            | 0.26                 | 0.11          | 5.26                   | 1.35          | 2.21             | 0.12          | 11.32  | 2.40          | 9.90        | 0.93          |
| NiO                            | nd                   | -             | nd                     | -             | nd               | -             | nd     | -             | nd          | -             |
| Na <sub>2</sub> O              | nd                   | -             | bdl                    | -             | bdl              | -             | bdl    | -             | 5.40        | 0.42          |
| K <sub>2</sub> O               | nd                   | -             | nd                     | -             | nd               | -             | nd     | -             | 0.34        | 0.09          |
| P                              | 0.03                 | 0.09          | bdl                    | -             | bdl              | -             | bdl    | -             | nd          | -             |
| S                              | 0.05                 | 0.27          | nd                     | -             | nd               | -             | nd     | -             | nd          | -             |
| Total                          | 99.50                | 0.81          | 98.71                  | 0.59          | 99.11            | 0.87          | 98.89  | 1.12          | 99.34       | 0.93          |
| Mg#                            | 48.88                | 14.29         | 61.03                  | 7.46          | 73.02            | 0.41          | 62.66  | 1.70          |             |               |
| Fe/Mn                          | 53.01                | 6.43          | 30.44                  | 2.79          | 28.84            | 2.80          | 28.53  | 3.19          |             |               |

|    |       |       |       |      |       |      |       |      |            |
|----|-------|-------|-------|------|-------|------|-------|------|------------|
| Fo | 48.88 | 14.29 |       |      |       |      |       |      |            |
| Wo |       |       | 11.11 | 2.94 | 4.43  | 0.24 | 24.08 | 5.51 |            |
| Fs |       |       | 34.55 | 6.21 | 25.79 | 0.34 | 28.39 | 3.35 |            |
| An |       |       |       |      |       |      |       |      | 49.30 4.42 |
| Ab |       |       |       |      |       |      |       |      | 48.66 3.95 |
| Or |       |       |       |      |       |      |       |      | 2.05 0.57  |

184 <sup>a</sup>The compositions of zoned olivine are averaged for modeling bulk mineral abundance. See text for  
 185 chemical zoning of olivine. <sup>b</sup>See Fig. 3 for compositions of zoned pigeonite. <sup>c</sup>Not determined. <sup>d</sup>Below detection  
 186 limit. <sup>e</sup>Includes Fe<sub>2</sub>O<sub>3</sub>.  
 187

### 188 3.1.1. Olivine

189 Olivine crystals in NWA 11115 are 250 μm to 2.5 mm in size and are mostly subhedral. All olivine grains show  
 190 some degree of chemical zonation from core to rim, although the larger crystals more strongly so (~Fo<sub>70</sub> to  
 191 Fo<sub>45</sub>); smaller olivine grains are much more ferroan (~Fo<sub>21</sub> to Fo<sub>35</sub>). Some larger olivine crystals appear to form  
 192 clumps or glomerophyres consisting of annealed crystals, and each sub-crystal contains its own distinct  
 193 chemical zonation from core to rims (Figure 2). We address the origin of the olivine crystals in §4.1.

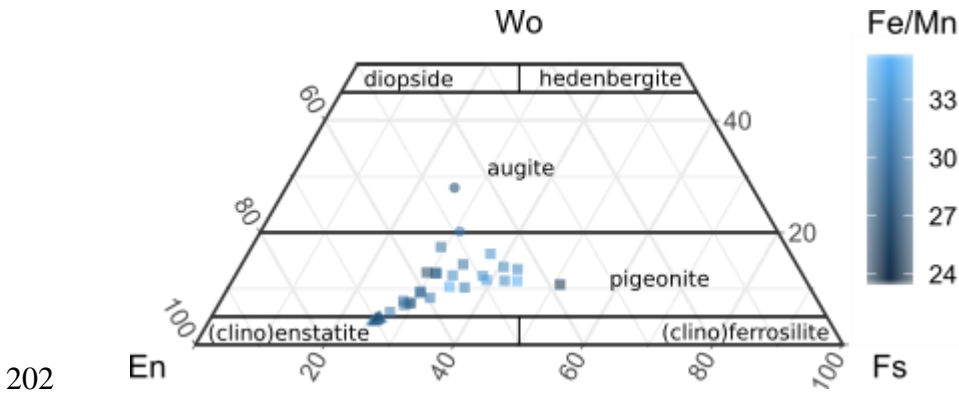


194 *Figure 2. False color composites of an olivine glomerophyre surrounded by maskelynite and pigeonite, and with numerous spinel grains. A) Red = iron, green = magnesium, blue = silicon. B) Cyan = calcium, yellow = sulfur, magenta = aluminum. Abundant calcite (arrows) infills fractures in the olivine phenocrysts, The scale bar is 2.5 mm across.*

### 196 3.1.2. Pyroxene

197 Most pyroxene crystals in the meteorite are subhedral to anhedral pigeonite, with grain sizes comparable  
 198 to the olivine grains, reaching up to ~2 mm in length. The pigeonite crystals are compositionally zoned from

199 core to rim (Figure 1 & Figure 2). Enstatite and augite are also present as accessory grains in the sample.  
 200 Analyzed pyroxene compositions are shown in Table 1 and Figure 3.  
 201

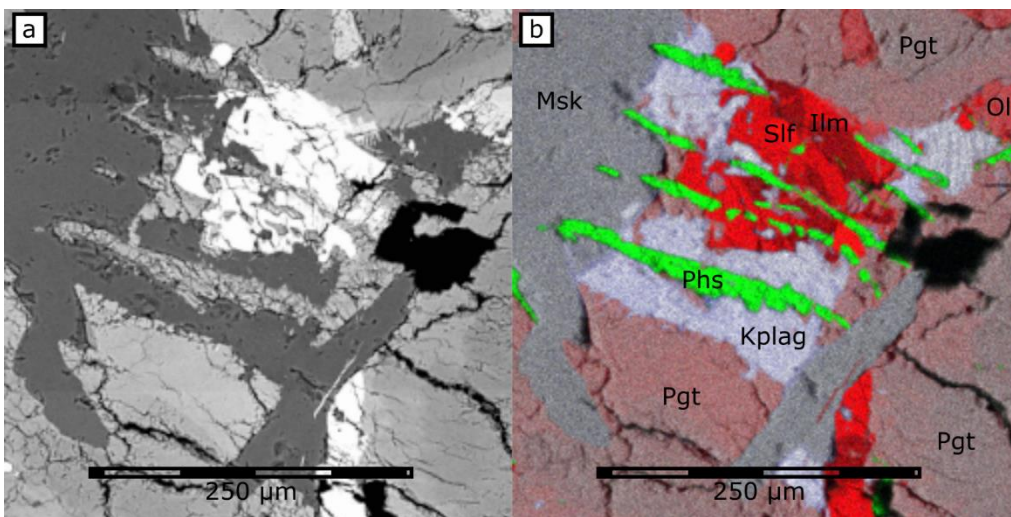


202  
 203  
 204  
 205  
 206  
 207  
 208  
 Figure 3. Compositional variability of the pyroxenes in NWA 11115. Darker points indicate lower Fe/Mn mass ratios and lighter points represent higher Fe/Mn mass ratios.

### 3.1.3. Maskelynite

204 Plagioclase feldspar in NWA 11115 is found in the form of maskelynite. Most of the plagioclase is K-poor (<  
 205 0.5 wt%) and does not exhibit substantial compositional variation (Table 1), however, some accessory K-  
 206 enriched plagioclase does occur (K ≈ 5–10 wt. %; Figure 4). These K-enriched alkali feldspar zones are most  
 207 often found adjacent to Ca-rich phosphate minerals and Cr-Fe-Ti-oxides (Figure 4).  
 208

209



209  
 210  
 Figure 4. Complex mineral intergrowths of K-rich plagioclase, phosphate, and Cr-Fe-Ti spinel. A) BSE image. B) False color composite. Red = iron, green = phosphorus, blue = potassium, background = silicon. Mineral abbreviations are: Msk = maskelynite, Kplag = K-rich plagioclase, Phs = phosphate, Pgt = pigeonite, Ol = olivine, Ilm = ilmenite, Slf =sulfide.

211 *3.1.1. Iron oxides and sulfides*

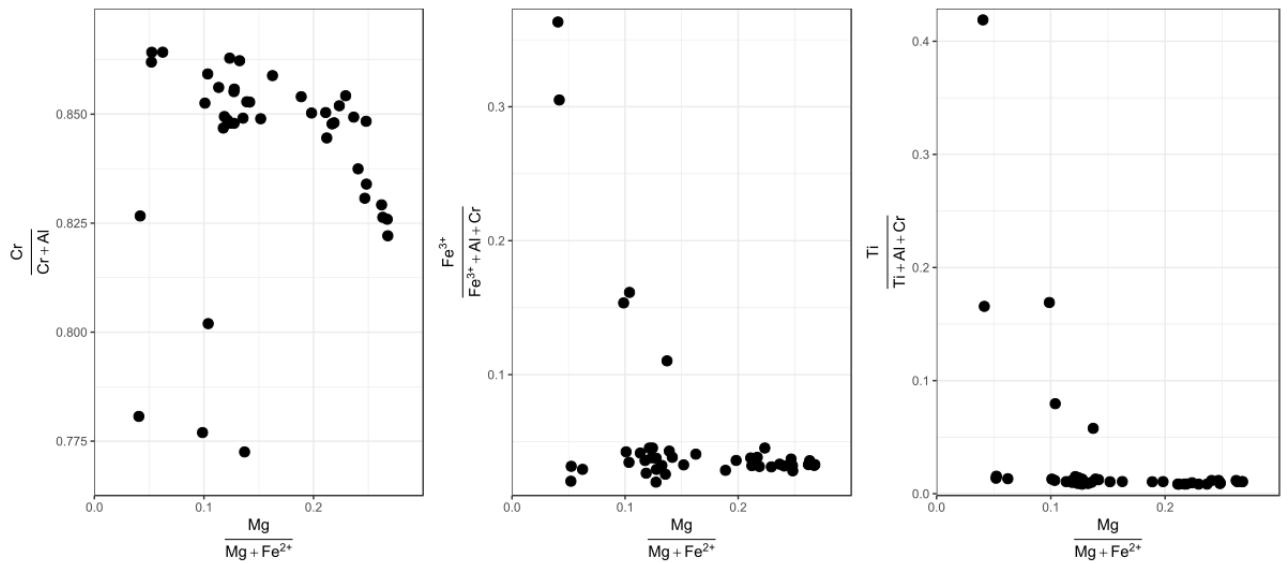
212 Spinel minerals are abundant throughout NWA 11115, poikilitically growing in olivine and pyroxene  
 213 grains, but also occurring separately adjacent to olivine and pyroxene grains. The spinel minerals are  
 214 intergrown magnesian chromite – hercynite – ulvöspinel solid solutions (Table 2 and Figure 5), that  
 215 occasionally also intergrow with sulfides (Figure 4). Individually measured compositions are therefore  
 216 variable, as for example in their TiO<sub>2</sub> concentration. Spinel grains with higher concentration of magnesium  
 217 also tend to have higher concentration of aluminum and lower concentration of chromium (Figure 5). Spinel  
 218 with higher concentration of Ti tend to occur in contact with phosphates and K-rich feldspar (Figure 4).  
 219

*Table 2. Composition of spinel group minerals in NWA 11115 (n = 42).*

|   | Wt. % |               |                   |               |
|---|-------|---------------|-------------------|---------------|
|   | Mean  | 25 % quartile | Median            | 75 % quartile |
| SiO <sub>2</sub>                            | 0.36  | 0.30          | 0.35              | 0.38          |
| TiO <sub>2</sub>                            | 1.68  | 0.69          | 0.77              | 0.89          |
| Al <sub>2</sub> O <sub>3</sub>              | 6.63  | 6.34          | 6.64              | 6.83          |
| Cr <sub>2</sub> O <sub>3</sub>              | 53.51 | 55.65         | 56.26             | 56.69         |
| V <sub>2</sub> O <sub>3</sub>               | 0.52  | 0.40          | 0.44              | 0.59          |
| Fe <sub>2</sub> O <sub>3</sub> <sup>a</sup> | 3.52  | 2.29          | 2.52              | 2.97          |
| FeO   | 29.38 | 26.69         | 29.38             | 30.03         |
| MnO   | 0.60  | 0.52          | 0.61              | 0.67          |
| MgO   | 3.12  | 2.27          | 2.68              | 4.31          |
| CaO   | 0.01  | 0             | 0                 | 0             |
| ZnO   | 0.14  | 0.01          | 0.11              | 0.24          |
| Total                                       | 99.46 | 99.18         | 99.52             | 99.82         |
|   |       |               | apfu <sup>c</sup> |               |
| Si  | 0.01  | 0.01          | 0.01              | 0.01          |
| Ti  | 0.05  | 0.02          | 0.02              | 0.02          |
| Al  | 0.28  | 0.27          | 0.28              | 0.28          |
| Cr  | 1.50  | 1.54          | 1.57              | 1.59          |
| V   | 0.01  | 0.01          | 0.01              | 0.02          |
| Fe <sup>3+</sup>                            | 0.09  | 0.06          | 0.07              | 0.08          |
| Fe <sup>2+</sup>                            | 0.87  | 0.79          | 0.88              | 0.89          |
| Mn  | 0.02  | 0.02          | 0.02              | 0.02          |
| Mg  | 0.16  | 0.12          | 0.14              | 0.23          |
| Ca  | 0.00  | 0.00          | 0.00              | 0.00          |
| Zn  | 0.00  | 0.00          | 0.00              | 0.01          |

|  |      |      |      |      |
|--|------|------|------|------|
| Total  | 3.00 | 3.00 | 3.00 | 3.00 |
| Atomic ratios  |      |      |      |      |
| Mg/(Mg+Fe <sup>2+</sup> )  | 0.16 | 0.12 | 0.14 | 0.22 |
| Cr/(Cr+Al)   | 0.84 | 0.83 | 0.85 | 0.85 |
| Fe <sup>3+</sup> /(Fe <sup>3+</sup> +Al+Cr)                                | 0.06 | 0.03 | 0.04 | 0.04 |
| Ti/(Ti+Al+Cr)  | 0.03 | 0.01 | 0.01 | 0.01 |
| Endmember molar composition <sup>d</sup>                                   |      |      |      |      |
| MgAl <sub>2</sub> O <sub>4</sub> <sup>e</sup>                              | 0.02 | 0.02 | 0.02 | 0.03 |
| FeAl <sub>2</sub> O <sub>4</sub> <sup>f</sup>                              | 0.12 | 0.11 | 0.12 | 0.12 |
| MgFe <sup>3+</sup> <sub>2</sub> O <sub>4</sub> <sup>g</sup>                | 0.01 | 0.00 | 0.01 | 0.01 |
| Fe <sup>2+</sup> Fe <sup>3+</sup> <sub>2</sub> O <sub>4</sub> <sup>h</sup> | 0.04 | 0.02 | 0.03 | 0.03 |
| MgCr <sub>2</sub> O <sub>4</sub> <sup>i</sup>                              | 0.12 | 0.09 | 0.11 | 0.18 |
| FeCr <sub>2</sub> O <sub>4</sub> <sup>j</sup>                              | 0.63 | 0.59 | 0.64 | 0.69 |
| MnCr <sub>2</sub> O <sub>4</sub> <sup>k</sup>                              | 0.01 | 0.01 | 0.01 | 0.02 |
| FeV <sub>2</sub> O <sub>4</sub> <sup>l</sup>                               | 0.01 | 0.00 | 0.01 | 0.01 |
| Fe <sub>2</sub> TiO <sub>4</sub> <sup>m</sup>                              | 0.02 | 0.01 | 0.01 | 0.01 |

220 <sup>a</sup>Calculated on the basis of stoichiometry, using the method of Droop (1987) implemented in Ferracutti et  
221 al. (2015). <sup>b</sup>Below detection limit. <sup>c</sup>Atoms per formula unit. <sup>d</sup>Calculated with the End-Members Generator  
222 (Ferracutti et al. 2015), for spinel group minerals with the formula  $X^{2+}Y^{3+}_2O_4$ , for a total charge of 8, normalized  
223 here to 1 mol. <sup>e</sup>Spinel. <sup>f</sup>Hercynite. <sup>g</sup>Magnesioferrite. <sup>h</sup>Magnetite. <sup>i</sup>Magnesiochromite. <sup>j</sup>Chromite.  
224 <sup>k</sup>Manganochromite. <sup>l</sup>Coulsonite. <sup>m</sup>Ulvöspinel.  
225



226

Figure 5. Compositional diversity in spinel group minerals analyzed in NWA 11115 ( $n = 42$ ). All spinel minerals analyzed are Cr-rich.

227

229 Phosphates in NWA 11115 consist primarily of subhedral, elongated (up to ~0.6 mm) and fractured  
 230 merrillite crystals, although minor amounts of chlorine-bearing apatite are also found in the sample (Table 3).  
 231 Phosphate crystals are typically found in contact with K-rich feldspar and Cr-Fe-Ti spinels (Figure 4).  
 232

Table 3. Phosphates in NWA 11115.

| Elements                           | Apatite                  | Merrillite  |               |
|------------------------------------|--------------------------|-------------|---------------|
|                                    | N = 1                    | N = 25      |               |
|                                    | Wt. %                    | Wt. %       | $\pm 1\sigma$ |
| O                                  | 39.63                    | 41.67       | 0.44          |
| Na                                 | bdl <sup>a</sup>         | 1.24        | 0.17          |
| Mg                                 | bdl                      | 1.37        | 0.12          |
| Al                                 | bdl                      | 0.01        | 0.03          |
| Si                                 | 0.24                     | 0.07        | 0.13          |
| P                                  | 18.62                    | 20.42       | 0.31          |
| S                                  | bdl                      | 0.02        | 0.11          |
| Cl                                 | 1.34                     | bdl         | nd            |
| Ca                                 | 37.85                    | 33.04       | 0.36          |
| Mn                                 | bdl                      | 0.02        | 0.05          |
| Fe                                 | 0.70                     | 2.31        | 0.25          |
| Total                              | 98.37                    | 100.10      | 0.99          |
| Calculated OH (= 100 – total – Cl) | 0.29                     | -           | -             |
|                                    | <i>apfu</i> <sup>b</sup> | <i>apfu</i> | $\pm 1\sigma$ |
| O <sup>c</sup>                     | 12                       | 28          | -             |
| Na                                 | 0                        | 0.58        | 0.08          |
| Mg                                 | 0                        | 0.61        | 0.05          |
| Al                                 | 0                        | 0           | 0.01          |
| Si                                 | 0.04                     | 0.03        | 0.05          |
| P                                  | 2.91                     | 7.09        | 0.06          |
| S                                  | 0                        | 0.01        | 0.04          |
| Cl                                 | 0.18                     | 0           | -             |
| Ca                                 | 4.58                     | 8.86        | 0.11          |
| Mn                                 | 0                        | 0           | 0.01          |
| Fe                                 | 0.06                     | 0.44        | 0.05          |
| Total +1 cations                   | 0                        | 0.58        | 0.08          |

$\Sigma$  +2 and +3 cations      4.64      9.92      0.09

233 <sup>a</sup>Below detection limit. <sup>b</sup>Atoms per formula unit. <sup>c</sup>Cations are normalized to the ideal number of oxygen atoms  
 234 per formula unit, i.e. 12 oxygen atoms in apatite (Ca<sub>5</sub>(PO<sub>4</sub>)<sub>3</sub>(F,Cl,OH)) and 28 oxygen atoms in merrillite  
 235 (Ca<sub>9</sub>NaMg(PO<sub>4</sub>)<sub>7</sub>).  
 236

237                    *3.1.3. Melt pockets*

238        The numerous melt pockets in NWA 11115 appear to be composed of a mixture of primary minerals.  
 239 Representative chemical analyses of three melt pockets are shown in Table 4. We used least-squares regression  
 240 to calculate the mixing ratio of each of the mineral components that form three representative melt pockets.  
 241 As mineral endmembers, we used the mean of the olivine, pyroxene (including enstatite, pigeonite and augite),  
 242 maskelynite, merrillite and spinel compositions of NWA 11115 that we report here (Table 1 to Table 3).  
 243 Additionally, we added stoichiometric pyrite as an endmember since we have not yet carried out detailed  
 244 analyses of the sulfide compositions in the meteorite. The results of the regression calculation are shown in  
 245 Table 4.  
 246

*Table 4. Compositional analyses of three melt pockets in NWA 11115, and results of the linear least-squares regression calculation to determine the proportion of mineral phase endmembers that form the melt pockets.*

|                                | Melt pocket 1    |                | Melt pocket 2 |                | Melt pocket 3 |                |
|--------------------------------|------------------|----------------|---------------|----------------|---------------|----------------|
|                                | N = 2            |                | N = 3         |                | N = 1         |                |
|                                | Wt. %            | $\pm 1\sigma$  | Wt. %         | $\pm 1\sigma$  | Wt. %         |                |
| SiO <sub>2</sub>               | 50.17            | 0.32           | 48.91         | 1.26           | 50.40         |                |
| TiO <sub>2</sub>               | 0.55             | 0.10           | 0.60          | 0.02           | 0.38          |                |
| Al <sub>2</sub> O <sub>3</sub> | 0.73             | 0.07           | 0.60          | 0.02           | 0.90          |                |
| Cr <sub>2</sub> O <sub>3</sub> | bdl <sup>a</sup> | -              | 0.32          | 0.09           | 0.36          |                |
| FeO <sub>T</sub> <sup>b</sup>  | 27.46            | 0.54           | 21.75         | 1.11           | 23.80         |                |
| MnO                            | 0.78             | 0.01           | 0.54          | 0.05           | 0.74          |                |
| MgO                            | 14.16            | 0.98           | 12.48         | 0.35           | 16.08         |                |
| CaO                            | 5.72             | 0.47           | 9.27          | 0.76           | 5.58          |                |
| Na <sub>2</sub> O              | bdl              | -              | 0.71          | 0.70           | bdl           |                |
| K <sub>2</sub> O               | bdl              | -              | bdl           | -              | bdl           |                |
| P                              | bdl              | -              | 1.22          | 0.02           | bdl           |                |
| S                              | bdl              | -              | 1.05          | 0.19           | bdl           |                |
| Total                          | 99.55            | 0.27           | 101.03        | 1.05           | 98.24         |                |
| Mg#                            | 47.86            | 2.23           | 50.58         | 1.96           | 54.64         |                |
| Linear regression              | Mixing ratio     | Standard Error | Mixing ratio  | Standard Error | Mixing ratio  | Standard Error |

|                            |      |      |      |      |      |      |
|----------------------------|------|------|------|------|------|------|
| Olivine                    | 0.26 | 0.17 | 0.01 | 0.16 | 0.14 | 0.10 |
| Pyroxene                   | 0.66 | 0.20 | 0.82 | 0.19 | 0.79 | 0.12 |
| Plagioclase                | 0.10 | 0.09 | 0.09 | 0.09 | 0.07 | 0.05 |
| Spinel                     | 0.00 | 0.05 | 0.01 | 0.05 | 0.01 | 0.03 |
| Merrillite                 | 0.01 | 0.03 | 0.06 | 0.04 | 0.01 | 0.02 |
| Pyrite                     | 0.03 | 0.05 | 0.06 | 0.04 | 0.02 | 0.03 |
| Adjusted<br>R <sup>2</sup> |      | 0.98 |      | 0.98 |      | 0.99 |

247 <sup>a</sup>Below detection limit. <sup>b</sup>Total Fe, including FeO and Fe<sub>2</sub>O<sub>3</sub>.

248

### 249 3.1. Bulk-rock geochemistry

250 Bulk sample chemistry of *Sample-UniBern* obtained by LA-ICP-MS (Table 5) revealed that NWA 11115 is  
 251 generally similar to other martian shergottites. Supplementary Table 1 contains the disregarded LA-ICP-MS  
 252 analysis carried out of *Sample-FMNH*, and an EMPA major element analysis on the same sample.

253 Bivariate Harker diagrams (Figure 6) allow for effective comparison of major element abundances between  
 254 NWA 11115 and other martian meteorites. The concentration of major oxides in NWA 11115 is consistent with  
 255 basaltic shergottites, apart from the MgO content, which lies between the average concentration in basaltic  
 256 shergottites and in olivine-phyric shergottites (Figure 6). The average magnesium number ( $100 \times \text{Mg}/(\text{Fe} +$   
 257  $\text{Mg})$ ) of NWA 11115 is  $\text{Mg}\# = 57.35$ . NWA 11115 shows an enriched REE pattern, similar to other enriched  
 258 shergottites, between NWA 856 and Los Angeles (Figure 7).

259

*Table 5. Whole rock chemistry of NWA 11115 Sample-UniBern, obtained by LA-ICP-MS from 27 repeat analyses. Oxides are reported in wt. %, and individual elements in  $\mu\text{g}/\text{g}$ . See Supplementary Information and Supplementary Spreadsheet File S1 for sidelined FMNH analyses and calibration measurements.*

|                                | Mean  | $\pm 2\sigma$ |
|--------------------------------|-------|---------------|
| SiO <sub>2</sub>               | 47.90 | 1.09          |
| TiO <sub>2</sub>               | 0.74  | 0.28          |
| Al <sub>2</sub> O <sub>3</sub> | 6.53  | 0.97          |
| FeO <sub>T</sub>               | 20.97 | 1.43          |
| MnO                            | 0.51  | 0.03          |
| MgO                            | 12.27 | 0.74          |
| CaO                            | 8.67  | 0.48          |
| Na <sub>2</sub> O              | 1.30  | 0.18          |
| K <sub>2</sub> O               | 0.18  | 0.04          |
| P <sub>2</sub> O <sub>5</sub>  | 0.73  | 0.21          |
| Li                             | 4.34  | 0.50          |

|    |         |         |
|----|---------|---------|
| Be | 0.37    | 0.15    |
| B  | 3.66    | 0.98    |
| Sc | 44.69   | 4.23    |
| V  | 232.17  | 41.30   |
| Cr | 2348.05 | 1560.64 |
| Co | 47.00   | 4.04    |
| Ni | 138.03  | 20.90   |
| Cu | 15.44   | 4.62    |
| Zn | 91.22   | 13.44   |
| Ga | 14.79   | 2.52    |
| Ge | 0.80    | 0.12    |
| As | 0.19    | 0.04    |
| Rb | 6.86    | 2.91    |
| Sr | 56.13   | 6.77    |
| Y  | 17.55   | 5.46    |
| Zr | 57.27   | 22.97   |
| Nb | 3.84    | 1.80    |
| Mo | 0.13    | 0.04    |
| Ag | 0.01    | 0.01    |
| Cd | 0.04    | 0.02    |
| In | 0.03    | 0.01    |
| Sn | 0.30    | 0.08    |
| Sb | 0.01    | 0.01    |
| Cs | 0.46    | 0.22    |
| Ba | 62.47   | 7.77    |
| La | 2.92    | 1.00    |
| Ce | 6.82    | 2.45    |
| Pr | 0.94    | 0.35    |
| Nd | 4.68    | 1.70    |
| Sm | 1.76    | 0.63    |
| Eu | 0.67    | 0.20    |
| Gd | 2.72    | 0.97    |
| Tb | 0.48    | 0.15    |
| Dy | 3.32    | 1.04    |
| Ho | 0.68    | 0.21    |
| Er | 2.01    | 0.58    |
| Tm | 0.26    | 0.07    |
| Yb | 1.76    | 0.42    |

|                   |       |       |
|-------------------|-------|-------|
| Lu                | 0.25  | 0.06  |
| Hf                | 1.69  | 0.60  |
| Ta                | 0.18  | 0.09  |
| W                 | 0.50  | 0.15  |
| Tl                | 0.03  | 0.01  |
| <sup>208</sup> Pb | 0.70  | 0.33  |
| Bi                | 0.004 | 0.003 |
| Th                | 0.51  | 0.14  |
| U                 | 0.13  | 0.02  |
| Mg#               | 57.35 | 1.68  |

260      <sup>a</sup>At or below the detection limit. Values represent maximum concentration measured.

261

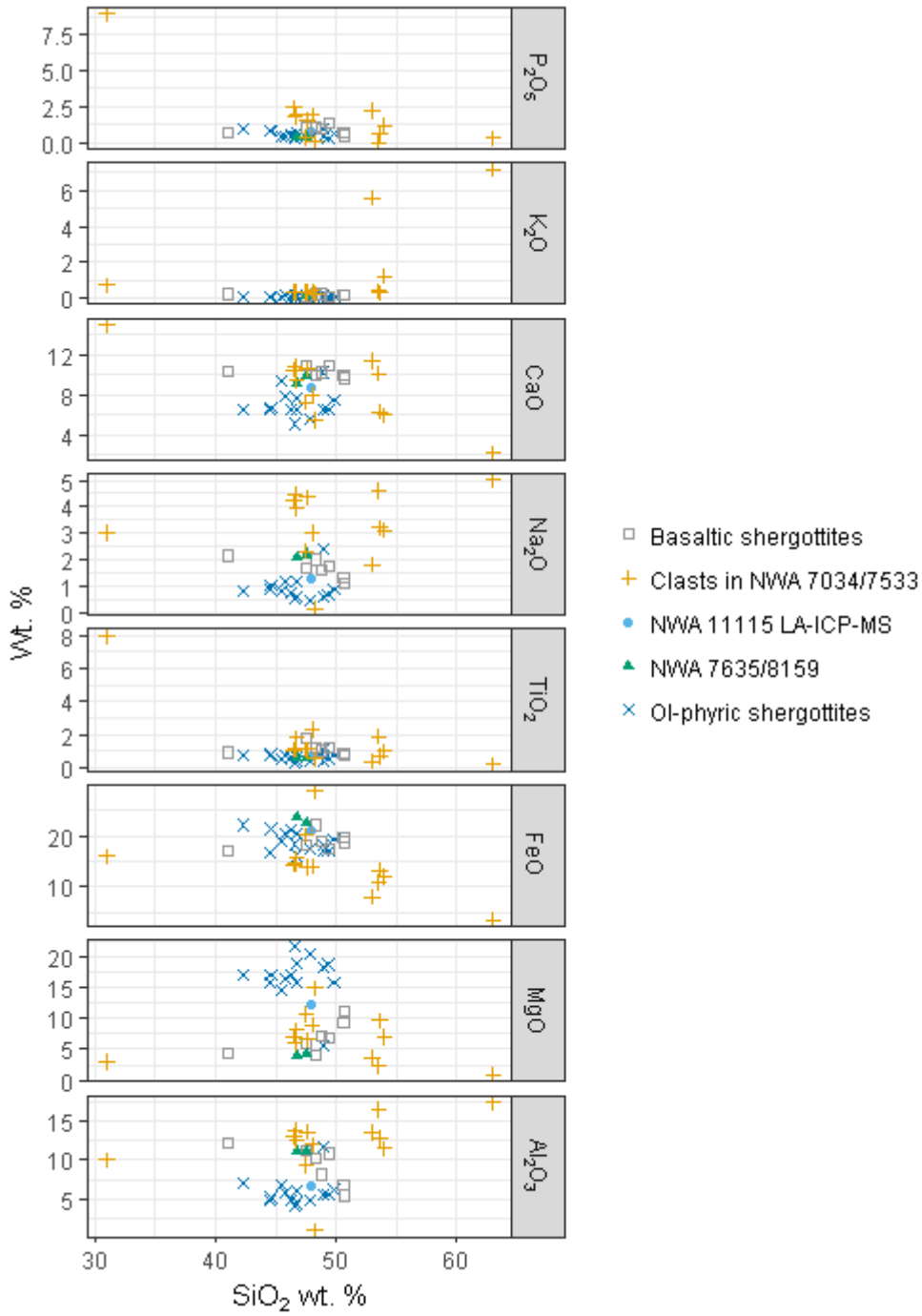


Figure 6. Harker diagram of major oxides in the bulk compositions of martian meteorites. Data for other meteorites are from the compilation by Filiberto (2017).

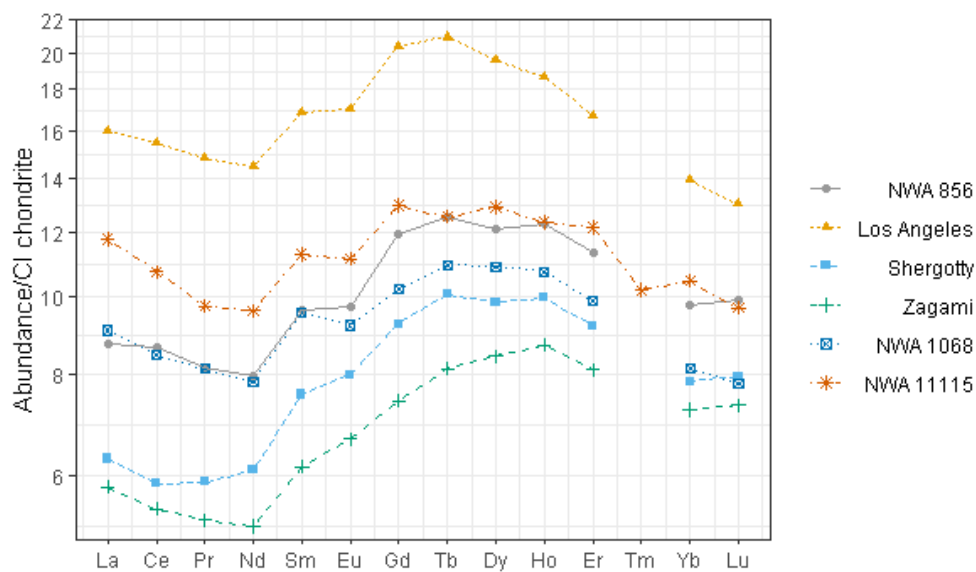
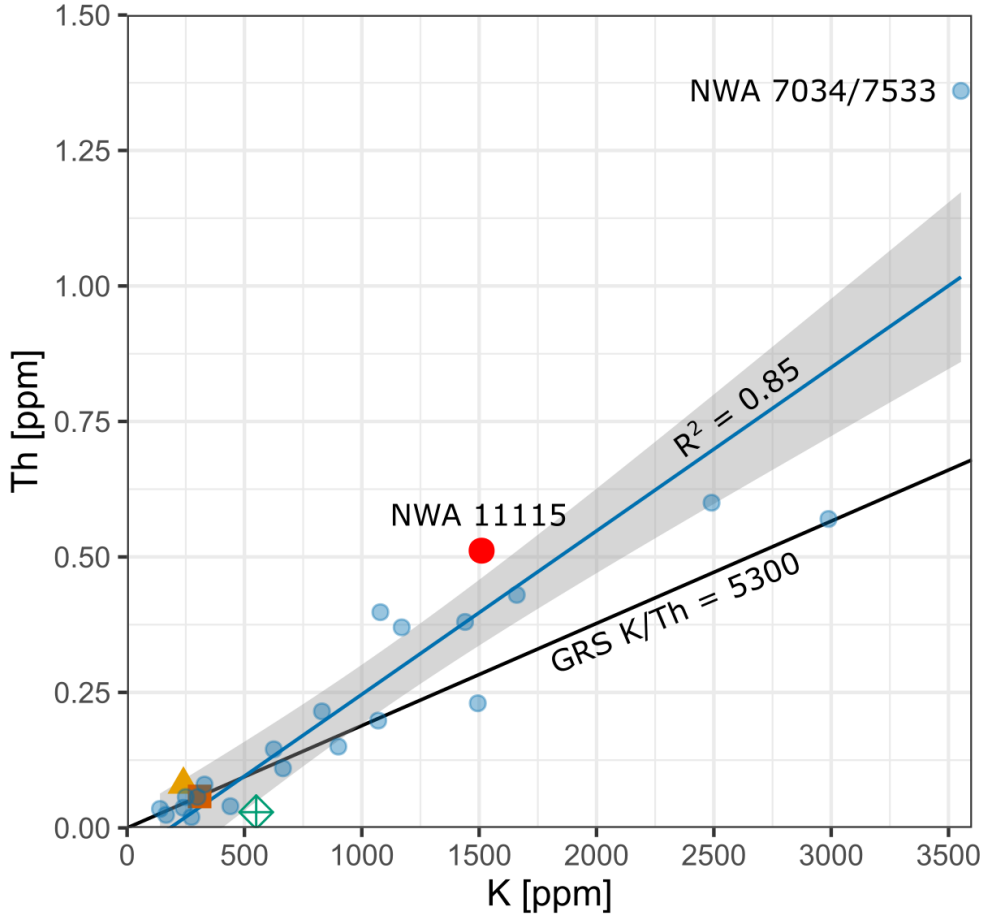


Figure 7. Rare earth element concentrations in enriched martian meteorites normalized to concentrations in CI chondrites. Data for CI chondrites are from the reported CI chondrite mean composition in Dauphas and Pourmand (2015), data for Shergotty and Zagami are from Barrat et al. (2001), and data for NWA 856 and Los Angeles are from the ICP-MS results by Jambon et al. (2002).



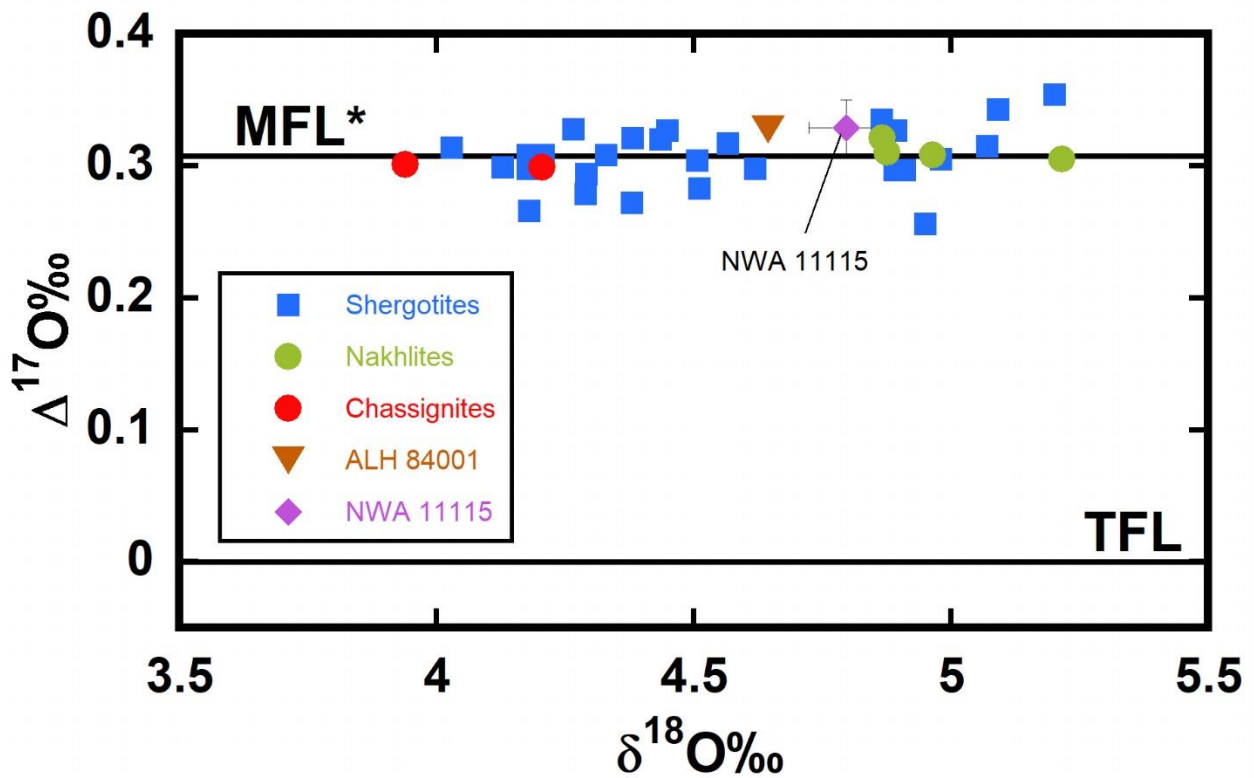
267

Figure 8. Comparison of  $K$  vs.  $Th$  concentration in NWA 11115 (red point), other martian meteorites (blue points), CI chondrites (green crossed diamond), bulk silicate Mars (orange square), bulk silicate Earth (yellow triangle) and Mars Odyssey's Gamma Ray Spectrometer measurements of the martian surface (black trend line). The blue line is a linear regression between all martian meteorites on the plot, apart from NWA 11115, and the grey area marks the 95 % confidence interval. Data for the martian meteorites apart from NWA 11115 are from the compilation by Filiberto (2017), CI chondrite data and bulk silicate Earth data are from McDonough and Sun (1995), and bulk silicate Mars is from Taylor (2013).

268

### 269 3.2. Oxygen isotopes

270 Laser-assisted fluorination of two aliquots of NWA 11115 gave an average isotopic composition of:  
 271  $\delta^{17}O = +2.823 \pm 0.017(2\sigma)$  ‰,  $\delta^{18}O = +4.796 \pm 0.072(2\sigma)$  ‰, and  $\Delta^{17}O = 0.329 \pm 0.021(2\sigma)$  ‰ (where  
 272  $\Delta^{17}O = \delta^{17}O - 0.52 \times \delta^{18}O$ ). The data for NWA 11115 are shown in relation to other martian meteorites  
 273 analyzed by laser fluorination (Fig. 6). The average  $\Delta^{17}O$  of these martian samples is 0.307 ‰, i.e., slightly  
 274 lower than the value obtained for NWA 11115 (Figure 9). However, the mean martian  $\Delta^{17}O$  value of Franchi  
 275 et al. (1999) is 0.321, i.e., closer to the value for NWA 1115. Thus, the oxygen isotope composition of NWA  
 276 11115 is consistent with it being a martian sample.



277

Figure 9. Oxygen isotope composition of NWA 11115 (error bars  $2\sigma$ ) and other martian meteorites analyzed by laser fluorination. MFL\* is the mean  $\Delta^{17}O$  of all the samples plotted in Fig. 6 with the exception of NWA 11115 and has a value of 0.307. TFL is the terrestrial fractionation line. Data: Franchi et al. (1999) and Meteoritical Bulletin Database oxygen isotope analyses for Tissint, DaG 478, DaG 670, JaH 479, LAR 06319, NWA 1669, NWA 2737, NWA 4222, NWA 5718, NWA 5790, NWA 6162, NWA 7032, NWA 7042, SaU 094, Y-000027, Y-000047, Y-000097.

278

#### 279 4. DISCUSSION

280 Concentrations of elements between martian meteorites can be compared to understand the provenance and  
 281 the relationship between martian rocks. Bulk element mass ratios of NWA 11115 (Fe/Mn, Na/Al, etc.) are  
 282 typical of other martian meteorites, and more specifically shergottites (Table 6) although the whole-rock K/Th  
 283 ratio ( $\sim 2987$ ) is significantly lower than the average surface of Mars (Taylor et al. 2006) and is also on the  
 284 lower end compared to other martian meteorites (Figure 8).

285

Table 6. Element mass ratios used for provenance tests. Martian meteorite average ratios from Taylor (2013) unless otherwise noted.

| Sample-UniBern |               | Martian meteorite mean |               |
|----------------|---------------|------------------------|---------------|
| Ratio          | $\pm 2\sigma$ | Ratio                  | $\pm 2\sigma$ |

Martian meteorite tests

|                     |         |        |   |                  |
|---------------------|---------|--------|---|------------------|
| Fe/Mn               | 41.4    | 1.7    | 40.3  | 2.3              |
| Ni ppm/Mg wt. %     | 18.649  | 2.465  | 17.946                                      | Nd               |
| K/Th                | 2987    | 810    | 5300 <sup>a</sup>                           | 220 <sup>a</sup> |
| P/Yb                | 1802.14 | 211.60 | 2065.27                                     | Nd               |
| Ga ppm/Al wt. %     | 4.284   | 0.625  | 4.067                                       | Nd               |
| Na/Al               | 0.278   | 0.015  | 0.247                                       | Nd               |
| MgO wt. %/Cu ppm    | 0.812   | 0.242  | 0.611                                       | Nd               |
| Shergottite tests   |         |        |   |                  |
| Rb/La               | 2.3822  | 1.0451 | 2.9066                                      | Nd               |
| Rb/K                | 0.0045  | 0.0012 | 0.0047                                      | Nd               |
| Cs/La               | 0.1613  | 0.0781 | 0.1805                                      | Nd               |
| Weathering tests    |         |        |   |                  |
| Th/U                | 4.09    | 0.77   | >0.2 (unweathered)<br><0.2 (weathered)      |                  |
| Sr/Nd               | 12.26   | 3.53   |   |                  |
| Ce/Ce <sup>*b</sup> | 1.01    | 0.04   | < 1 (leached)<br>> 1 (oxidized or enriched) |                  |
| K/La                | 526.94  | 154.59 |   |                  |

286 <sup>a</sup>Global surface average from the Gamma Ray Spectrometer on Mars Odyssey (Taylor et al. 2006).

287 <sup>b</sup>CI chondrite Ce abundance from Dauphas and Pourmand (2015).

288

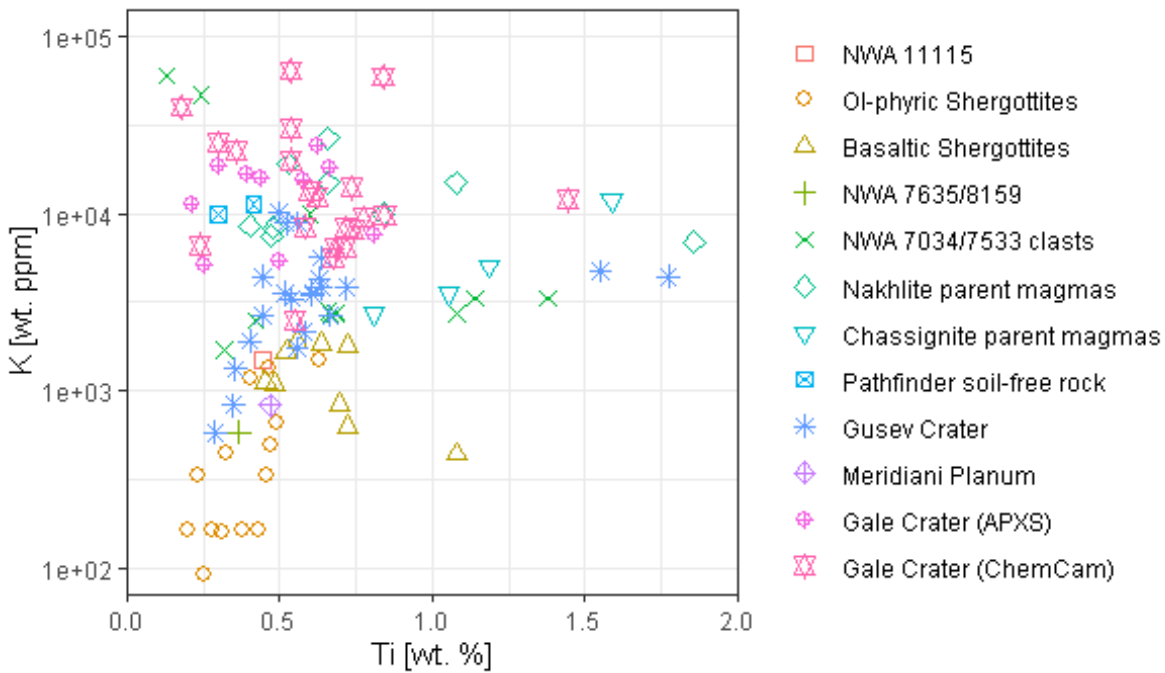
#### 289 **4.1. Provenance on Mars**

290 The relationship between Ti and K concentrations in martian meteorites and surface rocks on Mars has  
291 previously been used to discern between processes that affected the rocks on the path to crystallization, as well  
292 as post-crystallization processes such as metasomatism (e.g. Treiman and Filiberto, 2015; Filiberto, 2017).  
293 Similarly, the relationship of bulk MgO vs. bulk Al<sub>2</sub>O<sub>3</sub> also tracks the degree of igneous crystallization and  
294 accumulation processes, since earlier crystallizing phases (forsteritic olivine, Mg-pyroxene) tend to be richer  
295 in magnesium and poorer in aluminum, whereas later crystallizing phases (plagioclase feldspar) follow the  
296 opposite trend (e.g. Filiberto, 2017). NWA 11115 is somewhat closer to the olivine-phyric shergottites in its Ti  
297 vs. K relationship (Figure 10), but on the other hand, it is more in line with the basaltic shergottites, when  
298 comparing the relationship between MgO and Al<sub>2</sub>O<sub>3</sub> (Figure 11). From these relationships, we would assume  
299 that NWA 11115 crystallized relatively early on and did not experience much igneous fractionation (increasing  
300 Al<sub>2</sub>O<sub>3</sub>) or mantle metasomatism (increasing K; Schmidt et al. 2014). However, this is at odds with the  
301 moderately high bulk SiO<sub>2</sub> content (Figure 6 and Table 5), the large modal abundance of plagioclase feldspar  
302 within NWA 11115, as well as abundant phosphates, which typically form later in the crystallization sequence.  
303 Additionally, the highly enriched REE nature of the sample also appears to preclude early crystallization,  
304 unless the mantle source of NWA 11115 was especially REE-enriched.

305 Overall, the petrography and major element geochemistry closely resemble those of NWA 1068. NWA 1068 is  
 306 an olivine-phyric shergottite with a similar modal mineralogy, petrography and bulk geochemistry (Barrat et  
 307 al. 2002; Filiberto et al. 2010). The only significant differences between the meteorites appear to be the slightly  
 308 higher SiO<sub>2</sub> and lower MgO content of NWA 11115 (SiO<sub>2</sub> = 45.78 wt. % and MgO ≈ 16.64 wt. % for NWA  
 309 1068), which can be accounted for by the decreased olivine modal abundance in NWA 11115 relative to NWA  
 310 1068 (~14 % vs ~22%, Barrat et al. 2002). We note, however, that the bulk SiO<sub>2</sub> concentration was not reported  
 311 for NWA 1068 by Barrat et al. (2002), but estimated by Filiberto et al. (2010). Thus, the petrologic experiments  
 312 by Filiberto et al. (2010) for NWA 1068 apply to NWA 11115 also: all the olivine in the meteorite are likely to  
 313 be settled cumulate crystals, and NWA 11115 probably originated in the same magmatic event close to, or  
 314 slightly above the NWA 1068 in the cumulate pile, which would be consistent with the somewhat more REE-  
 315 enriched chemistry and differences in modal mineralogy.

316 The analyzed melt pockets are intriguing in that their compositions consistently undersample the plagioclase  
 317 composition of NWA 11115: while the meteorite is composed of ~ 30 vol. % maskelynite, the melt pockets  
 318 appear to be composed of < 10 wt. % maskelynite (as is apparent from the low Al<sub>2</sub>O<sub>3</sub>; Table 4) and > 66 wt. %  
 319 pyroxene (Table 4), which, even accounting for the lower density of plagioclase relative to pyroxene, is a  
 320 significant mismatch. In addition, the melting temperature of plagioclase is lower than that of pyroxene, so the  
 321 plagioclase composition should form a larger mass fraction of the melt pockets, unless shock melting is favored  
 322 by frictional heating along the grain boundaries of the large phenocrysts, i.e. olivine and pyroxene. Frictional  
 323 heating as the main mechanism for melt production would be consistent with the feathered texture along olivine  
 324 and pyroxene grains where melt pockets are found.

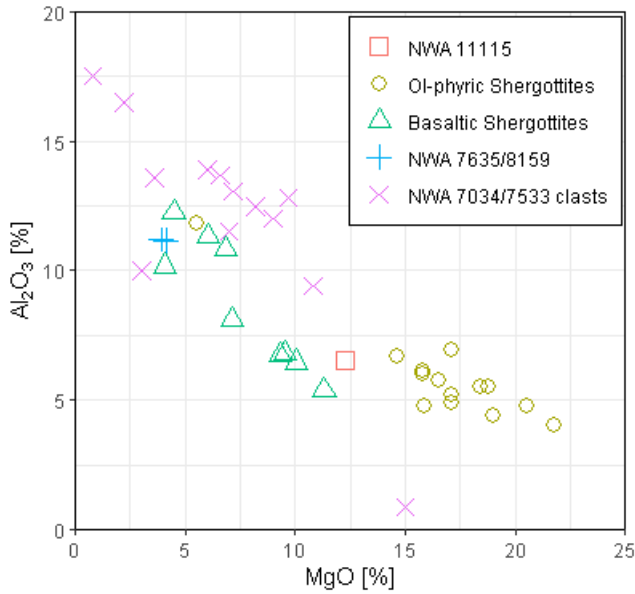
325



326

Figure 10. Semilog graph of bulk Ti concentration (wt. %) vs. bulk K concentration (wt. ppm). Data adapted from Filiberto (2017), with new data for NWA 11115. A data point from a Fe-Ti-P-rich clast of NWA 7034 is not plotted, as it contains high Ti concentration and lies far from the center of the graph.

327



328

Figure 11. Bulk MgO wt. % vs. bulk Al<sub>2</sub>O<sub>3</sub> wt. % in NWA 11115 and other martian meteorites. Data for meteorites other than NWA 11115 are from the compilation by Filiberto (2017).

329

#### 330 4.2. Terrestrial weathering

331 Bulk Th/U, Sr/Nd, and K/La mass ratios are often used as proxies for the degree of weathering meteorites  
 332 experienced during their residence on Earth (e.g. Barrat et al. 2001; Taylor 2013; Taylor et al. 2002), measuring  
 333 the relative excess of aqueously mobile versus immobile elements. Preferential depletion or enrichment of  
 334 cerium is also a common result of terrestrial weathering in meteorites (Croaz et al. 2003; e.g. Floss and Croaz  
 335 1991, 1993), which either causes the removal of Ce<sup>3+</sup> by dissolution of REE-rich phases (e.g. Ca-phosphates),  
 336 or oxidizes the relatively soluble Ce<sup>3+</sup> to relatively insoluble Ce<sup>4+</sup>, thereby enriching Ce in the sample relative  
 337 to REEs with similar masses (La and Pr). We quantify Ce concentration anomalies, by calculating the “Ce/Ce\*”  
 338 ratio as in Dauphas and Pourmand (2015):

$$\frac{\text{Ce}}{\text{Ce}^*} = \frac{\text{Ce}_N}{\text{La}_N^{0.48} \times \text{Pr}_N^{0.52}} \quad (1)$$

339 where Ce<sub>N</sub>, La<sub>N</sub>, and Pr<sub>N</sub> are the concentrations of these REE elements in the sample normalized to the  
 340 concentrations of these in CI chondrites. (We use the CI chondrite values reported in Dauphas and Pourmand  
 341 (2015).)

342 By these measures, NWA 11115 is, if at all, only slightly affected by terrestrial weathering: the Th/U ratio is  
 343 near-chondritic, the relatively high Sr is tracked by high Nd, and the Ce/Ce\* ratio is close to 1 (Table 6). In  
 344 addition, the bulk oxygen isotopes place the meteorite far from the terrestrial fractionation line (Figure 9).  
 345 However, the meteorite clearly contains an abundance of large fractures infilled with calcite (e.g. Figure 2) and

346 other secondary phases, so the discrepancy is puzzling. A possible explanation is that the alteration was largely  
347 isochemical, requiring only atmospheric water to react with the mineral phases in the meteorite to form the  
348 alteration phases, the positive and negative Ce anomalies balance out, and the absence of a terrestrial oxygen  
349 signature could be attributed to the preparation procedure of the sample for laser-assisted fluorination. This is  
350 an unsatisfying explanation, however, because the CO<sub>2</sub> required to form the carbonates was likely atmospheric,  
351 and not indigenous to the meteorite. We note that abundant martian carbonates are found in the Allan Hills  
352 84001 meteorite and some nakhlite meteorites (e.g. Lafayette, Nakhla, Governador Valadares, e.g. Bridges et  
353 al., 2019). However, we argue that the alteration phases are likely terrestrial because the calcite-filled fractures  
354 cross-cut the fusion crust (see CT scan in the electronic appendix). Future targeted analyses of the carbon  
355 isotopes in the calcite could more conclusively determine their origin.

356

## 357 **5. CONCLUSIONS**

358 NWA 11115 is an enriched olivine-phyric shergottite with some unusual properties, but is otherwise  
359 petrographically and geochemically similar to NWA 1068, albeit with a higher concentration of SiO<sub>2</sub> as a result  
360 of higher maskelynite modal abundance at the expense of cumulate olivine crystals. The bulk K/Th ratio of  
361 NWA 11115 is low (K/Th  $\approx$  2987) compared to other martian meteorites (Figure 8), and the surface of Mars  
362 (K/Th  $\approx$  5300 (Taylor et al. 2006)). This could be related to fractional crystallization, as in some Zagami  
363 lithologies (McCoy et al. 1999). However, the K abundance is not especially low compared to other martian  
364 meteorites. Instead, NWA 11115 is Th enriched. Most likely, the large phosphate crystals are the hosts of the  
365 Th (as well as U, also relatively enriched). We recommend further analyses of the phosphate minerals, which  
366 we also suspect are the main hosts of the REE. Given the similarity of NWA 1068 with NWA 11115, we suggest  
367 that these meteorites are genetically linked, with NWA 11115 somewhat higher up in the cumulate pile  
368 suggested by its higher REE-enrichment, and the differences in modal mineralogy mentioned above. In  
369 addition, the analyzed melt pockets in NWA 11115 are intriguing because their compositions undersample the  
370 abundant maskelynite in the meteorite (Table 4). Finally, while NWA 11115 is likely altered, as evidenced by  
371 the abundant fracture-filling calcite, trace element proxies for alteration (e.g. Sr/Nd) do not correlate with other  
372 martian meteorites known to have experienced hot desert alteration (e.g. Dhofar 019 and Dar al Gani 476/489;  
373 see Folco et al. 2000; Taylor et al. 2002). Further analyses of the alteration mineralogy are an area of interest  
374 to understand its provenance and effects on the geochemistry of the meteorite.

375

### 376 **Data Availability**

377 All data are available in the Supplementary Information file, and at the following Zotero link: [\[DOI and link  
378 to be made live after review\]](#).

379

### 380 **Acknowledgements**

381 The authors acknowledge T. Boudreaux for donating NWA 11115 to the Field Museum, J. Greer and J. Holstein  
382 for help with sample preparation, L. Kööp and B. Strack for SEM support, S. Rastegar for preliminary SEM

383 analysis, L. Dussubieux for LA-ICP-MS support, A. I. Neander and Z.-X. Luo for  $\mu$ CT scanning and support,  
384 and J. Filiberto and A. Treiman for useful discussions. We thank Thomas Pettke for assistance with LA-ICP-  
385 MS analyzes of the pressed powder pellets at the University of Bern. GPS Division analytical facilities at  
386 Caltech and Chi Ma are thanked for the support on EMPA analysis. PRH acknowledges support from the  
387 Tawani Foundation. MMD's portion of the work was done partly as a private venture and not in the author's  
388 capacity as an employee of the Jet Propulsion Laboratory, California Institute of Technology. The authors  
389 declare no competing interests.

390

## 391 **References**

392

393 Agee C. B. et al. 2013. Unique Meteorite from Early Amazonian Mars: Water-Rich Basaltic Breccia  
394 Northwest Africa 7034. *Science* 339:780–785.

395 Barrat J. A., Blichert-Toft J., Nesbitt R. W., and Keller F. 2001. Bulk chemistry of Saharan shergottite Dar al  
396 Gani 476. *Meteoritics & Planetary Science* 36:23–29.

397 Barrat J. A., Jambon A., Bohn M., Gillet P. h, Sautter V., Göpel C., Lesourd M., and Keller F. 2002.  
398 Petrology and chemistry of the Picritic Shergottite North West Africa 1068 (NWA 1068).  
399 *Geochimica et Cosmochimica Acta* 66:3505–3518.

400 Borg L. E., and Draper D. S. 2003. A petrogenetic model for the origin and compositional variation of the  
401 martian basaltic meteorites. *Meteoritics & Planetary Science* 38:1713–1731.

402 Bridges J. C., Hicks L. J., and Treiman A. H. 2019. Chapter 5 - Carbonates on Mars. In *Volatiles in the*  
403 *Martian Crust*, edited by Filiberto J., and Schwenzer S. P. Elsevier. pp. 89–118  
404 <http://www.sciencedirect.com/science/article/pii/B9780128041918000052>.

405 Crozaz G., Floss C., and Wadhwa M. 2003. Chemical alteration and REE mobilization in meteorites from hot  
406 and cold deserts. *A Special Issue Dedicated to Robert M Walker* 67:4727–4741.

407 Dauphas N., and Pourmand A. 2015. Thulium anomalies and rare earth element patterns in meteorites and  
408 Earth: Nebular fractionation and the nugget effect. *Geochimica et Cosmochimica Acta* 163:234–261.

409 Droop G. T. R. 1987. A general equation for estimating Fe<sup>3+</sup> concentrations in ferromagnesian silicates and  
410 oxides from microprobe analyses, using stoichiometric criteria. *Mineralogical Magazine* 51:431–  
411 435.

412 Ferracutti G. R., Gargiulo M. F., Ganuza M. L., Bjerg E. A., and Castro S. M. 2015. Determination of the  
413 spinel group end-members based on electron microprobe analyses. *Mineralogy and Petrology*  
414 109:153–160.

415 Filiberto J., Musselwhite D. S., Gross J., Burgess K., LE L., and TREIMAN A. H. 2010. Experimental  
416 petrology, crystallization history, and parental magma characteristics of olivine-phyric shergottite  
417 NWA 1068: Implications for the petrogenesis of “enriched” olivine-phyric shergottites. *Meteoritics*  
418 *& Planetary Science* 45:1258–1270.

419 Filiberto J., and Dasgupta R. 2011. Fe<sup>2+</sup>–Mg partitioning between olivine and basaltic melts: Applications to  
420 genesis of olivine-phyric shergottites and conditions of melting in the Martian interior. *Earth and*  
421 *Planetary Science Letters* 304:527–537.

422 Filiberto J., Gross J., Trela J., and Ferré E. C. 2014. Gabbroic Shergottite Northwest Africa 6963: An  
423 intrusive sample of Mars. *American Mineralogist* 99:601.

- 424 Filiberto J. 2017. Geochemistry of Martian basalts with constraints on magma genesis. *Chemical Geology*  
425 466:1–14.
- 426 Floss C., and Crozaz G. 1991. Ce anomalies in the LEW85300 eucrite: evidence for REE mobilization  
427 during Antarctic weathering. *Earth and Planetary Science Letters* 107:13–24.
- 428 Floss C., and Crozaz G. 1993. Heterogeneous REE patterns in oldhamite from aubrites: Their nature and  
429 origin. *Geochimica et Cosmochimica Acta* 57:4039–4057.
- 430 Folco L., Franchi I. A., D’Orazio M., Rocchi S., and Schultz L. 2000. A new martian meteorite from the  
431 Sahara: The shergottite Dar al Gani 489. *Meteoritics & Planetary Science* 35:827–839.
- 432 Franchi I. A., Wright I. P., Sexton A. S., and Pillinger C. T. 1999. The oxygen-isotopic composition of Earth  
433 and Mars. *Meteoritics & Planetary Science* 34:657–661.
- 434 Goodrich C. A. 2002. Olivine-phyric martian basalts: A new type of shergottite. *Meteoritics & Planetary*  
435 *Science* 37:B31–B34.
- 436 Greenwood R. C., Burbine T. H., Miller M. F., and Franchi Ian. A. 2017. Melting and differentiation of early-  
437 formed asteroids: The perspective from high precision oxygen isotope studies. *Geochemistry* 77:1–  
438 43.
- 439 Gross J., Filiberto J., Herd C. D. K., Melwani Daswani M., Schwenzer S. P., and Treiman A. H. 2013.  
440 Petrography, mineral chemistry, and crystallization history of olivine-phyric shergottite NWA 6234:  
441 A new melt composition. *Meteoritics & Planetary Science* 48:854–871.
- 442 Humayun M. et al. 2013. Origin and age of the earliest Martian crust from meteorite NWA 7533. *Nature*  
443 503:513–516.
- 444 Irving A. J. 2021. An up-to-date List of Martian Meteorites. <https://imca.cc/mars/martian-meteorites-list.htm>  
445 (Accessed May 28, 2021).
- 446 Jambon A., Barrat J. A., Sautter V., Gillet Ph., Göpel C., Javoy M., Joron J. L., and Lesourd M. 2002. The  
447 basaltic shergottite Northwest Africa 856: Petrology and chemistry. *Meteoritics & Planetary Science*  
448 37:1147–1164.
- 449 McCoy T. J., Wadhwa M., and Keil K. 1999. New lithologies in the Zagami meteorite: evidence for  
450 fractional crystallization of a single magma unit on Mars. *Geochimica et Cosmochimica Acta*  
451 63:1249–1262.
- 452 McDonough W. F., and Sun S. -. 1995. The composition of the Earth. *Chemical Evolution of the Mantle*  
453 120:223–253.
- 454 McSween H. Y. 1994. What we have learned about Mars from SNC meteorites. *Meteoritics* 29:757–779.
- 455 Melwani Daswani M., Heck P. R., Greber N. D., and Greenwood R. C. 2017. Petrography and Geochemistry  
456 of Northwest Africa 11115: A New, Enriched, High Thorium Basaltic Shergottite. In *80th Annual*  
457 *Meeting of the Meteoritical Society*. p. 6302.
- 458 Miller M. F., Franchi I. A., Sexton A. S., and Pillinger C. T. 1999. High precision  $\delta^{17}\text{O}$  isotope  
459 measurements of oxygen from silicates and other oxides: method and applications. *Rapid*  
460 *Communications in Mass Spectrometry* 13:1211–1217.
- 461 Papike J. J., Karner J. M., Shearer C. K., and Burger P. V. 2009. Silicate mineralogy of martian meteorites.  
462 *Geochimica et Cosmochimica Acta* 73:7443–7485.
- 463 Peters D., and Pettke T. 2017. Evaluation of Major to Ultra Trace Element Bulk Rock Chemical Analysis of

- 464 Nanoparticulate Pressed Powder Pellets by LA-ICP-MS. *Geostandards and Geoanalytical Research*  
465 41:5–28.
- 466 Santos A. R., Agee C. B., McCubbin F. M., Shearer C. K., Burger P. V., Tartèse R., and Anand M. 2015.  
467 Petrology of igneous clasts in Northwest Africa 7034: Implications for the petrologic diversity of the  
468 martian crust. *Geochimica et Cosmochimica Acta* 157:56–85.
- 469 Schindelin J. et al. 2012. Fiji: an open-source platform for biological-image analysis. *Nature Methods* 9:676–  
470 682.
- 471 Schmidt M. E. et al. 2014. Geochemical diversity in first rocks examined by the Curiosity Rover in Gale  
472 Crater: Evidence for and significance of an alkali and volatile-rich igneous source. *Journal of*  
473 *Geophysical Research: Planets* 119:64–81.
- 474 Starkey N. A. et al. 2016. Triple oxygen isotopic composition of the high- $^3\text{He}/^4\text{He}$  mantle. *Geochimica et*  
475 *Cosmochimica Acta* 176:227–238.
- 476 Taylor L. A. et al. 2002. Martian meteorite Dhofar 019: A new shergottite. *Meteoritics & Planetary Science*  
477 37:1107–1128.
- 478 Taylor G. J. et al. 2006. Variations in K/Th on Mars. *Journal of Geophysical Research: Planets* 111:E03S06.
- 479 Taylor G. J. 2013. The bulk composition of Mars. *Chemie der Erde - Geochemistry* 73:401–420.
- 480 The Meteoritical Society. 2017. *Meteoritical Bulletin 106*, Lunar and Planetary Institute  
481 <https://www.lpi.usra.edu/meteor/> (Accessed August 28, 2018).
- 482 Treiman A. H. 1996. The perils of partition: Difficulties in retrieving magma compositions from chemically  
483 equilibrated basaltic meteorites. *Geochimica et Cosmochimica Acta* 60:147–155.
- 484 Treiman A. H., and Filiberto J. 2015. Geochemical diversity of shergottite basalts: Mixing and fractionation,  
485 and their relation to Mars surface basalts. *Meteoritics & Planetary Science* 50:632–648.
- 486 Usui T., McSween H. Y., and Floss C. 2008. Petrogenesis of olivine-phyric shergottite Yamato 980459,  
487 revisited. *Geochimica et Cosmochimica Acta* 72:1711–1730.
- 488 Wittmann A., Korotev R. L., Jolliff B. L., Irving A. J., Moser D. E., Barker I., and Rumble D. 2015.  
489 Petrography and composition of Martian regolith breccia meteorite Northwest Africa 7475.  
490 *Meteoritics & Planetary Science* 50:326–352.
- 491